JOURNAL OF AIRCRAFT
Vol. 46, No. 6, November–December 2009

Behaviors of Vortex Wake in Random Atmospheric Turbulence

Z. C. Zheng* and Ying Xu†
Kansas State University, Manhattan, Kansas 66506
and
D. K. Wilson‡
U.S. Army, Hanover, New Hampshire 03755

DOI: 10.2514/1.44288

Atmospheric turbulence has significant influences on both the trajectories and strengths of wake vortices. In this paper, a quasi-wavelet method is used to generate a random atmospheric turbulence field based on the von Kármán spectrum, in which atmospheric turbulence is represented by groups of random eddies. An inviscid wake vortex system, out-of-ground effect or in-ground effect, is immersed in the generated turbulence background to study the effects of random turbulence on wake vortices. The simulated wake trajectories are compared with literature data from several current prediction models as well as from field measurement.

I. Introduction

AIRCRAFT wake vortices residing in terminal areas impose severe flight control demands in congested airports. Therefore, predicting their positions and strengths is very important to terminal flight operations. There are several currently considered state-of-the-art wake vortex prediction models, both in the United States and in Europe. However, according to the recent reviews by the National Transportation Safety Board and the National Research Council [1], these models do not yet provide capabilities that are sufficiently robust when compared with actual field measurement data, because of the simplified assumptions used in the models. These simplified assumptions are represented in modeling wake vortex initialization (including aircraft types and configurations), wake vortex in-ground effect, and atmospheric conditions (including wind, stratification, and turbulence). Particularly, the stochastic behavior of background turbulence is not included. Here, we address this issue for the purpose of building new probabilistic capabilities for wake prediction.

The fast-time prediction models include the deterministic models APA, TDAWP, D2P, and VFS, and the most-known probabilistic model, P2P [2–10]. These models are derived, more or less, from Greene's model [11]. There are some other models before these models and they are mostly reviewed by Spalart [12].

The drawback of the current probabilistic models, such as P2P [7–9] and other probabilistic analysis models [13], is that they are actually based on deterministic models, along with the statistics of measured data. In these models, the background turbulence is only represented by the measured eddy-dissipation rate (EDR) in the circulation decay model. That is, each EDR is used in a deterministic fashion for vortex decay, although with statistical variations based on curve-fitting the measured data. However, for realistic atmospheric turbulence, it is well known that each EDR is a result of a random turbulent velocity field. (Hence, it is called a turbulent flow.) Such randomness obviously generates corresponding random behaviors of wake vortices, changes the trajectories of wake vortices, and deforms the wake vortices. These random behaviors directly influence the probability of wake hazard posed by wake vortices in the flight path of a following aircraft. To address this issue, we use a quasi-wavelet model to generate a random turbulent background velocity based on EDR with the von Kármán spectrum for typical atmospheric turbulence. Quasi-wavelets (QWs) form a representation of turbulence consisting of self-similar eddylike structures with random orientations and positions in space. As the size of these eddies is comparable with that of the wake vortices, they can drastically influence the wake vortices. The QW-generated turbulence is thus used as background turbulence in a vortex method to address the atmospheric effects on wake vortex behaviors.

II. Quasi-Wavelet Method for Random Atmospheric Turbulence

The atmospheric velocity field can be decomposed into mean and fluctuation parts:

$$\mathbf{V} = \bar{\mathbf{V}} + \mathbf{V} \tag{1}$$

where $\mathbf{V}$ is the total velocity, $\bar{\mathbf{V}}$ is the mean background flow velocity, and $\mathbf{V}'$ is the turbulent velocity fluctuation. The mean background velocity is the part included in the current literature models, but not the fluctuation velocity part. The argument could be that all the models just tried to model the mean behavior of wake vortices, and the fluctuation part was therefore averaged out. The flaw of this argument is that the mean behavior of wake vortices is at a different scale than the mean behavior of the atmosphere. It is true that all the current models are intended to capture the mean behavior of wake vortices. The mean behavior is with respect to the scale of wake vortices, and therefore only the wake-generated turbulence is averaged out. Atmospheric turbulence, however, is external to the wake vortices, which does not include the part of turbulence generated by the wake vortices themselves. It is at a different scale and is usually larger than the wake-generated turbulence. If we consider the averaging process as a filter, then the wake vortex model is based on a filter that filters out higher-frequency fluctuation than most of the background turbulence. In other words, the background turbulence, such as low-frequency fluctuations, survives such a filter. The scale of the background turbulence can be comparable with that of the mean behavior of the wake vortices. For example, the length scale of atmospheric turbulence near the inertial subrange and the energy-containing subrange can be in the range of a few meters to several hundred meters [14]. Apparently, at this size of the length scale, atmospheric turbulence is able to directly transport wake vortices in both horizontal and vertical directions, with its velocity fluctuations at the magnitude possibly comparable with the mean wind speed.

Now the question is how to obtain velocity fluctuations of atmospheric turbulence. From a theoretical point of view, velocity

Received 10 March 2009; revision received 24 June 2009; accepted for publication 26 June 2009.

*Associate Professor, Department of Mechanical and Nuclear Engineering. AIAA Senior Member.
†Graduate Research Assistant, Department of Mechanical and Nuclear Engineering.
‡Research Physical Scientist, Signature Physics Branch, Cold Regions Research and Engineering Laboratory.

fluctuations of turbulence can be calculated by direct numerical simulation of atmospheric turbulent flow, but this is not a practical approach even with today's state-of-the-art computing power. A practical approach is to use measured information, such as EDR, to approximately construct velocity fluctuations based on known turbulence spectra, such as the von Kármán spectrum. Here, we use a QW method to develop a random velocity field for wake vortex simulation. Other models [15] that generate turbulence for computational simulation can possibly be used as well.

In a quasi-wavelet representation of turbulence, self-similar eddylike structures are used with random orientations and positions in space. Such a representation is based on a spatially localized parent function that is related to the turbulent kinetic energy spectrum. The orientations and positions of the QWs are randomly generated. The QW basis functions are not required to be mutually orthogonal or to form a mathematically complete set.

In the QW method, each QW can be viewed as a random eddy. The fluctuation velocity field created by the QWs (or the QW ensembles) is found at a spatial location $\mathbf{r}$ by superposition of these eddies:

$$\mathbf{V}'(\mathbf{r}) = \sum_{\alpha=1}^{N} \sum_{n=1}^{N_\alpha} \mathbf{v}^{\alpha n}(\mathbf{r}) \tag{2}$$

where N is the number of size classes, N_α is the number of QWs for the size class α, and the velocity field associated with each QW is

$$\mathbf{v}^{\alpha n}(\mathbf{r}) = \boldsymbol{\Omega}^{\alpha n} \times \mathbf{f}(\mathbf{r} - \mathbf{b}^{\alpha n}) \tag{3}$$

where $\boldsymbol{\Omega}^{\alpha n}$ is the angular velocity vector of the QW, $\mathbf{b}^{\alpha n}$ is the center of the QW, and $\mathbf{f}$ is the QW parent function to be determined by the expression of turbulence energy spectrum. The randomness of the resultant velocity fluctuations is that the orientation of the QWs, the direction of vectors $\boldsymbol{\Omega}^{\alpha n}$, and their eddy centers $\mathbf{b}^{\alpha n}$ are random variables. They are generated using random-number generators in the computer. The strength of the eddy is determined by the size of eddy and the EDR in the inertial subrange. Note that turbulence generated by the QW method is a solenoidal field and therefore satisfies the incompressible flow condition.

We use the von Kármán spectrum to represent atmospheric turbulence, because it contains the Kolmogorov spectrum (inertial subrange) in the high-wave-number limit and is also valid for the lower wave numbers comprising the energy subrange. The expression for the von Kármán energy spectrum is

$$E(k) = C \frac{\sigma_v^2 k^4 L_v^5}{(1 + k^2 L_v^2)^{17/6}} \tag{4}$$

where C is a von Kármán spectrum constant, σ_v is the velocity scale, and L_v is the length scale near the transition between the energy and inertial subranges and is proportional to the distance from the ground in shear turbulence. The detailed mathematical derivation of the QW representation of the von Kármán spectrum is given by Goedecke et al. [16] and Wilson et al. [17], and a typical resultant eddy structure and spectrum are shown in Fig. 1. The z direction is the vertical distance from the ground. The structure is represented by vorticity isosurface, with the shading representing the velocity magnitude of eddies. It can be seen that the length scale of turbulence becomes larger when the vertical distance from the ground increases. It also shows that the eddies can sometimes be fairly strong, shown as hot spots of atmospheric turbulence. When a wake vortex system is immersed in these eddies, they transport and deform the vortices in a random fashion.

III. Effects of Random Atmospheric Turbulence on Two-Dimensional Wake Vortex Trajectories

Here, we consider a vortex wake system that can be represented by a pair of counter-rotating point vortices. The trajectories of each of the vortices is expressed as

$$\frac{\mathrm{d}\mathbf{X}_i}{\mathrm{d}t} = \mathbf{V}_i + \mathbf{u}_i \tag{5}$$

where $\mathbf{X}_i$ represents the position vector of each of the vortices and $\mathbf{V}_i$ and $\mathbf{u}_i$ are the background and induced velocities, respectively, at the position of each of the vortices, and $\mathbf{V}_i$ can be further decomposed into mean and fluctuation parts, as shown in Eq. (1). In this study, we assume that the mean background flow is the crosswind and that turbulence fluctuations are provided by the QW representation. A two-dimensional wake vortex system in a y–z plane (with the x direction being the vortex axial direction) in proximity to the ground is shown in Fig. 2. With inviscid ground effects in in-ground-effect (IGE) cases, we have

$$\frac{\mathrm{d}Y_i}{\mathrm{d}t} = \bar{V} + V' + v_i \tag{6}$$

$$\frac{\mathrm{d}Z_i}{\mathrm{d}t} = \bar{W} + W' + w_i \tag{7}$$

where $\bar{V}$, V', $\bar{W}$, and W' are the mean and fluctuation crosswind velocities in the y and z directions, respectively, and $i = 1$ or 2, representing each of the two vortices in the wake, with

$$Y_1(t=0) = -Y_2(t=0) = b_0/2$$

$$Z_1(t=0) = Z_2(t=0) = h_0$$

$$\Gamma_1(t=0) = -\Gamma_2(t=0) = \Gamma_0$$

and the induced velocities

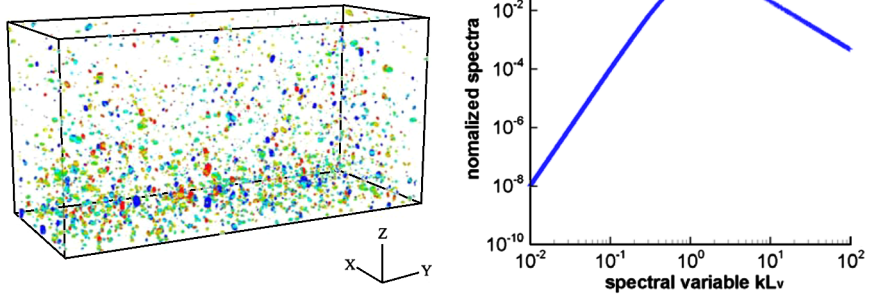

a) Vorticity isosurface b) Energy spectrum

Fig. 1 Eddy structures of the QW representation of atmospheric turbulence with the von Kármán energy spectrum and normalized energy spectrum of the von Kármán turbulence. The color represents the velocity magnitude. The size of the simulation box is 15 m (x) by 50 m (y) by 15 m (z).

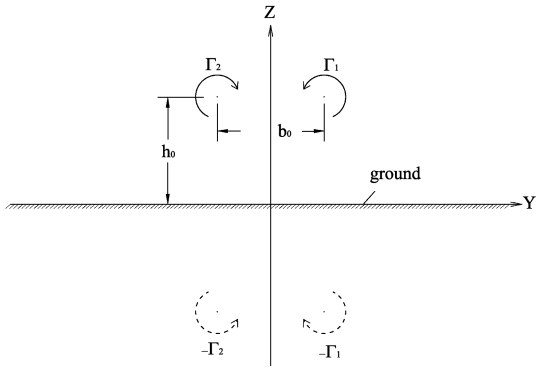

Fig. 2 A pair of wake vortices in proximity to the ground.

$$v_i = \frac{\Gamma_i}{4\pi Z_i} + \frac{\Gamma_j}{2\pi}\left[\frac{Z_i + Z_j}{(Y_i - Y_j)^2 + (Z_i + Z_j)^2} - \frac{Z_i - Z_j}{(Y_i - Y_j)^2 + (Z_i - Z_j)^2}\right] \tag{8}$$

$$w_i = \frac{\Gamma_j}{\pi}\frac{2(Y_i - Y_j)Z_i Z_j}{[(Y_i - Y_j)^2 + (Z_i + Z_j)^2][(Y_i - Y_j)^2 + (Z_i - Z_j)^2]} \tag{9}$$

where i, $j = 1$ or 2 (no summation with respect to i or j in the preceding expressions). In out-of-ground-effect (OGE) cases, the induced velocities change to

$$v_i = -\frac{\Gamma_j}{2\pi}\frac{Z_i - Z_j}{(Y_i - Y_j)^2 + (Z_i - Z_j)^2} \tag{10}$$

$$w_i = \frac{\Gamma_j}{2\pi}\frac{Y_i - Y_j}{[(Y_i - Y_j)^2 + (Z_i - Z_j)^2]} \tag{11}$$

Note that the mean positions of vortices are expressed in Eqs. (6) and (7) with the wind velocity fluctuations V' and W' to be zero.

Near the ground, the wind speed is assumed to follow a velocity distribution of a turbulent boundary with the logarithmic profile:

$$U = \frac{U^*}{\kappa}\ell_n\frac{z}{z_0} \tag{12}$$

In this paper, the turbulent boundary-layer friction speed U^* is selected as 0.5 m/s; z_0, the roughness height, is selected as 0.1 m; and κ is the von Kármán constant to be 0.4. In a neutrally stratified atmosphere, the EDR can be expressed as [18]

$$\varepsilon = \frac{(U^*)^3}{\kappa z} \tag{13}$$

In the current QW atmospheric turbulence model, we modify the preceding equation to be

$$\varepsilon = \frac{(U^*)^3}{\kappa \max(z, z_0, \Delta z)} \tag{14}$$

where Δz is the grid size that indicates the smallest size of QW eddies to be resolved in the simulation and is selected to be 0.2 m. The largest size of eddies in a particular vertical layer is 1.8 times the height in the z direction [19]. Therefore, the largest eddy size of overall QW computation becomes 90 m. The number of QW size classes is determined by the largest and smallest eddies to be resolved at each vertical layer. The packing factor is 0.005 in each class. The simulated vorticity field of atmospheric turbulence is shown in Fig. 1.

According to Sarpkaya [20], under a turbulent atmosphere with neutral stratification, the circulation decay follows:

$$\frac{\Gamma_i}{\Gamma_0} = \exp\left[-C\frac{t\Gamma_0}{2\pi b_0^2 T_c^*}\right] \tag{15}$$

where C is a constant of 0.45; Γ_0 and b_0 are, respectively, the initial circulation and vortex span; and T_c^* is a function of ε^*, a dimensionless eddy-dissipation rate of atmospheric turbulence defined as

$$\varepsilon^* = \frac{2\pi b_0}{\Gamma_0}(\varepsilon b_0)^{1/3} \tag{16}$$

The relations between T_c^* and ε^* vary depending on the value of eddy-dissipation rate and are listed by Sarpkaya et al. [5]. For the domain size and the wake vortex parameters used in this study, the eddy-dissipation rate in the entire range can be approximately related to T_c^* as [5]

$$\varepsilon^*(T_c^*)^{4/3} = 0.7475 \tag{17}$$

A. OGE Results

We simulate two OGE cases and compare them with the results from the fast-time models of Sarpkaya [5,20], D2P, and TDAWP [21]. These two cases are under neutral stratification, have no mean crosswind ($\bar{V} = \bar{W} = 0$), and represent, respectively, a low-turbulence and a high-turbulence environment. For the low-turbulence case, $\varepsilon = 10^{-4}$ m^2/s^3, and for the high-turbulence case, $\varepsilon = 10^{-2}$ m^2/s^3. The QW turbulence in OGE cases is thus generated based on a constant EDR instead of on Eq. (14).

The simulated vortex trajectories are generated by integrating Eqs. (6) and (7) in time, with the initial conditions of $h_0 = 300$ m, $b_0 = 50$ m, and $\Gamma_0 = 575$ m^2/s. A Runge–Kutta second-order time-marching scheme is used for time integration, with a time step of 0.004 s to reach a total integration time of 200 s. The circulation decay follows Sarpkaya's [5,20] decay model equation (15) throughout the entire integration time.

Figures 3 and 4 are the simulation results using 101 random realizations of QW turbulence, in comparison with fast-time predictions of Sarpkaya [5,20], TDAWP, and D2P for the low- and high-turbulence cases. Because the decay model we use follows Sarpkaya model, in the low-turbulence case, both the altitude and circulation decay histories are close to those of Sarpkaya's model. Because the EDR is considered constant in the OGE cases, the decay history in our simulation is still the same as that of Sarpkaya's model even in the high-turbulence case. However, the altitude history is different from the Sarpkaya model prediction in the high-turbulence case, because of the velocity in the random background turbulence. In fact, the range of random altitude histories is approximately those of D2P and TDAWAS. It also should be noted that at an early time, results of all the fast-time models and different realizations of QW simulation are very close to each other. At a later time, there are more differences among the fast-time models and more deviations of different realizations of the QW simulation results. That means that the uncertainty of different fast models increases with time, which is due to the influence of random turbulence. The influence of random turbulence also explains increased deviations in the QW simulation results when time increases. Comparing the two turbulence levels, the uncertainty also increases when turbulence intensity increases.

B. IGE Results

The run 9 case of the Idaho Falls tower flyby test campaign [22] has previously been used as a benchmark case for verifying wake vortex IGE models [21,23]. In the run 9 case, a B757-200 flew by the 61 m (200 ft) tower at an altitude of 70 m (h_0). The initial wake vortex span and circulation for the B757-200 were $b_0 = 29.8$ m and $\Gamma_0 = 362.8$ m^2/s [23]. Wake vortices were measured using a laser Doppler velocimetry lidar and a monostatic acoustic velocimeter system, and in the following discussion we do not distinguish the data measured by the two different devices, although the quality of the data by different devices could be different. Weather data with

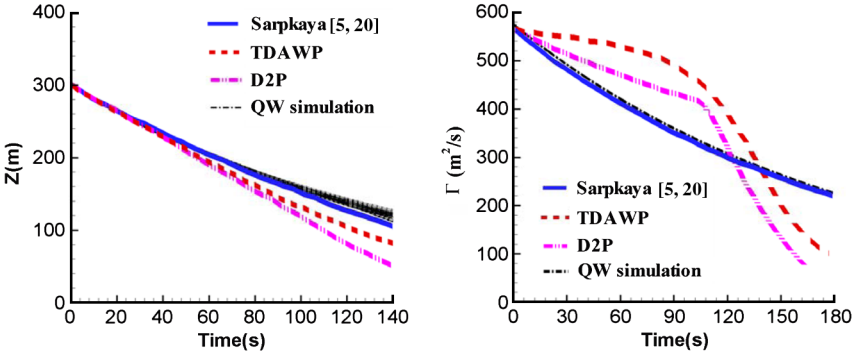

a) Altitude history b) Circulation decay history

Fig. 3 Histories of low-turbulence simulation.

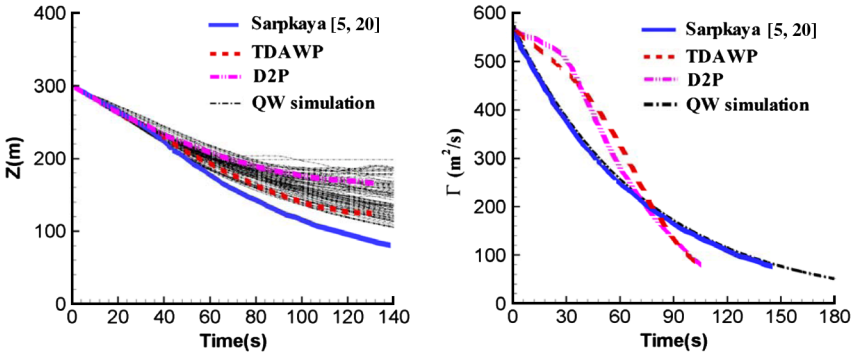

a) Altitude history b) Circulation decay history

Fig. 4 Histories of high-turbulence simulation.

relatively high vertical resolution were measured from the tower and tethersonde. For the near-ground crosswind velocity profile, the logarithmic distribution (12) reasonably fits the velocity sounding data, with friction speed of 0.5 m/s and roughness height of 0.1 m, as shown in Fig. 5, although with a friction speed of 0.7 m/s fitting the higher-altitude data better. Then atmospheric turbulence is generated by the QW method using the EDR value calculated from Eq. (14). The number of realizations of random turbulence used in the run 9 case simulation is 202: twice that used in the OGE cases. Further increasing the number of random turbulence realizations does not significantly change the statistical range of the simulation results.

For vortex trajectories, we compare the results with those from Idaho Falls measurement data, Navier–Stokes (N-S) simulation [23], large eddy simulation (LES) (using TASS), and fast-time models of Sarpkaya [5,20] and TDAWP [21]. Figure 6 is the comparisons for vortex trajectories of both upstream and downstream (or upwind and downwind, which are in the reference to the flow direction of crosswind) vortices. The general trend is that the upstream vortex simulation has better agreement with the measurement than the downstream vortex simulation. This is due to the fact that the crosswind shear has a more significant effect on the downstream vortex than the upstream vortex [21,23], which also results in a weaker secondary ground vortex under the upstream vortex than the downstream vortex. For the upstream vortex trajectory, all the models underpredict the vortex rebound from the ground, with the N-S simulation giving the closest result to the measurement and the TDAWP model giving the most underpredicting altitude. The QW simulation still underpredicts the rebound; however, it covers the range of prediction results from N-S, LES, Sarpkaya [5,20], and TDAWP and has a trend to include the measurement data within the deviation range. However, the N-S and LES results provide good predictions for the downstream vortex trajectory, because they are able to include crosswind shear in a most physically sound way among all the models. The TDAWP model performs better than Sarpkaya, which significantly underpredicts vortex rebound. The QW simulation results are between TDAWP and Sarpkaya and still underpredict the rebound altitude. It should be pointed out that in the current QW simulation, there are no secondary ground vortices included and the ground surface is only an inviscid surface. But even without that effect, it seems that the vortex rebound, due to image vortices and turbulence, can still be simulated by the QW model. Moreover, these effects can be comparable with those of secondary vortices and crosswind shear to cause vortex rebound.

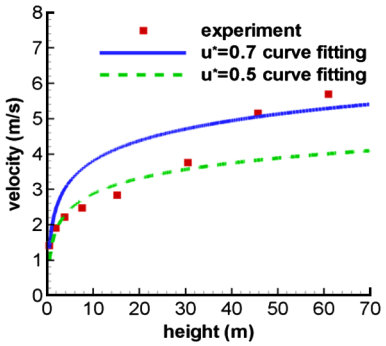

Fig. 5 Measured velocity profile and logarithmically fitted surface wind velocity profiles using Eq. (12) for run 9.

Figure 7 shows comparisons for circulation decay histories. As there is no circulation data from other fast-time models, we compare with measurement and N-S simulation data of Ash and Zheng [23]. For both upstream and downstream vortices, the decay is closely matched by the QW simulation at earlier time, which is even better that the N-S simulation. For the upstream vortex, starting at 60 s, the QW simulation underpredicts the circulation value, although after 110 s it seems that the predicted trend is again getting closer to that of the measurement. For the downstream vortex, both the N-S simulation and QW simulation overpredict the circulation value starting at 20 s. However, the range of the QW simulation starts to get close to measurement at 60 s, which is also better than the N-S prediction.

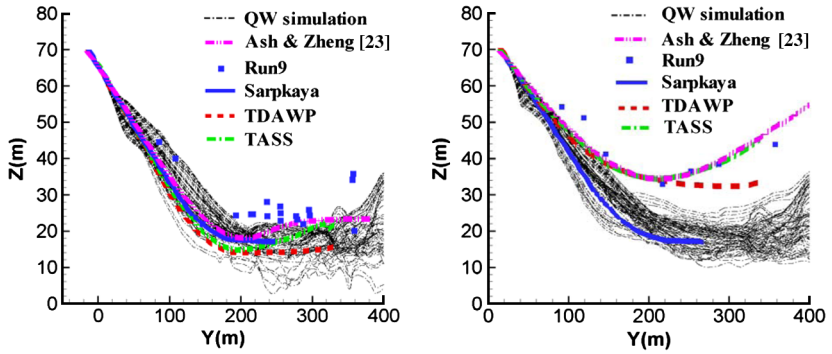

a) Upstream vortex trajectory b) Downstream vortex trajectory

Fig. 6 Run 9 wake vortex trajectories.

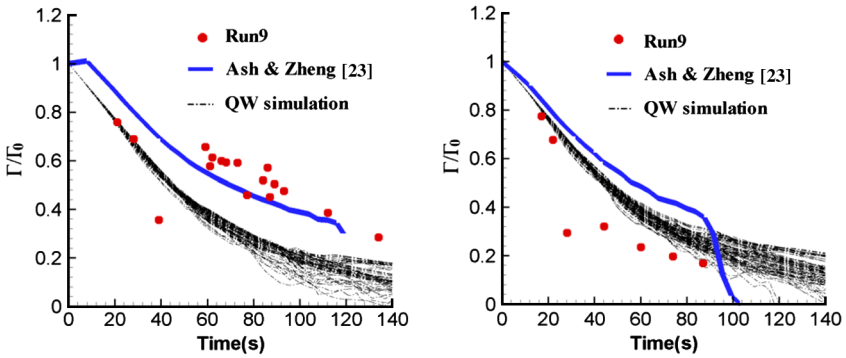

a) Upstream vortex decay b) Downstream vortex decay

Fig. 7 Run 9 wake vortex circulation decay histories.

The trajectory and circulation decay behaviors shown in Figs. 6 and 7 provide the evidence that the significance of the random background turbulence needs to be taken into consideration at the same level as that of secondary vortices from the viscous ground effect and strong stratification [24–26]. This is because the results show that random turbulence is able to significantly transport wake vortices, leading to a random range of decay and trajectory histories showing vortex rebound and tilt. These behaviors of wake vortices can also be caused by secondary ground vortices and strong stratification, although they are not included in the current QW simulation. In a three-dimensional wake, atmospheric turbulence is the source to trigger sinusoidal instabilities in the vortex wake system [27–29], a topic deserving further study.

We should note that although three-dimensional effects are not included in the current model, some of the disparity between the measured data and simulation could also be caused by three-dimensional effects. In two-dimensional simulation, the vortices are assumed to be straight lines with an infinitely long length. As the effects of vortex burst and sinusoidal instability (either long wave or short wave) are intrinsically three-dimensional, these phenomena are unable to be accurately included in any two-dimensional models. In addition, aerodynamics of a gusty environment on a stationary aircraft may not suffice to fully address the effects of atmospheric turbulence on the vortex wake of a flying aircraft.

IV. Conclusions

In this paper, a random atmospheric turbulence field of the von Kármán spectrum is generated with a QW method. A wake vortex system of both OGE and IGE is immersed in the generated turbulence. The simulation results are compared with measurement data and literature results from other fast-time models and N-S and LES simulations. In the QW simulation, circulation decay follows Sarpkaya's [5,20] EDR decay model. The crosswind effect is included in vortex trajectory histories, and the inviscid ground effect is considered. For a particular weather condition, a few hundreds of realizations of random QW turbulence provide a statistically stable range of wake vortex behaviors. For the OGE cases, circulation decay histories from the QW simulation are the same as what the Sarpkaya model predicts, and trajectories cover the range contoured by predictions from the models of Sarpkaya, TDAWP, and D2P. For the IGE cases, by comparing the results of a benchmark case of Idaho Falls run 9, it shows that the QW trajectories cover the range of those predicted by fast-time models of Sarpkaya and TDAWP and by N-S and LES simulations when the crosswind shear is not strong. The QW circulation decay predictions follow the general decay trend of the measured data and can even perform better than some N-S simulations. The range of uncertainty produced by the QW simulation increases with time and intensity of turbulence, which is a truly physical property of this kind of statistical model.

References

[1] "Wake Turbulence: An Obstacle to Increased Air Traffic Capacity" National Academy of Sciences, Washington, D.C., 2008.

[2] Robins, R. E., Delisi, D. P., and Greene, G. C., "Algorithm for Prediction of Trailing Vortex Evolution," *Journal of Aircraft*, Vol. 38, No. 5, 2001, pp. 911–917. doi:10.2514/2.2851

[3] Robins, R. E., and Delisi, D. P., "NWRA AVOSS Wake Vortex Prediction Algorithm Version 3.1.1," NASA CR-2002-211746, 2002.

[4] Robins, R. E., and Delisi, D. P., "Wake-Vortex Algorithm Scoring Results," NASA CR-2002-211745. 2002.

[5] Sarpkaya, T., Robins, R. E., and Delisi, D. P., "Wake Vortex Eddy-Dissipation Model Predictions Compared with Observations," *Journal of Aircraft*, Vol. 38, No. 4, 2001, pp. 687–692. doi:10.2514/2.2820

[6] Proctor, F., Hamilton, D., and Switzer, G., "TASS Driven Algorithm for Wake Prediction," 44th AIAA Aerospace Sciences Meeting and Exhibit, AIAA Paper 2006-1073, Reno, NV, 2006.

[7] Holzäpfel, F., and Holzapfel, F., "Probabilistic Two-Phase Wake Vortex Decay and Transport Model," *Journal of Aircraft*, Vol. 40, No. 2, 2003, pp. 323–331. doi:10.2514/2.3096

[8] Holzäpfel, F., and Robins, R. E., "Probabilistic Two-Phase Wake Vortex Decay Model: Application and Assessment," *Journal of Aircraft*, Vol. 41, No. 5, 2004, pp. 1117–1126. doi:10.2514/1.2280

[9] Holzäpfel, F., "Probabilistic Two-Phase Wake Vortex Model: Further Development and Assessment," *Journal of Aircraft*, Vol. 43, No. 3, 2006, pp. 700–708. doi:10.2514/1.16798

[10] Winckelmans, G., Duquesne, T., Treve, V., Desenfans, O., and Bricteux, L., "Summary Description of the Models Used in the Vortex Forecast System (VFS)," Univ. Catholique de Louvain, Louvain-la-Neuve, Belgium, Apr. 2005.

[11] Greene, G. C., "An Approximate Model of Vortex Decay in the Atmosphere," *Journal of Aircraft*, Vol. 23, No. 7, 1986, pp. 566–573. doi:10.2514/3.45345

[12] Spalart, P. R., "Airplane Trailing Vortices," *Annual Review of Fluid Mechanics*, Vol. 30, 1998, pp. 107–138. doi:10.1146/annurev.fluid.30.1.107

[13] Shortle, J., and Jeddi, B., "Using Multilateration Data in Probabilistic Analysis of Wake Vortex Hazard for Landing Aircraft," *Transportation Research Record*, 2007, pp. 90–96. doi:10.3141/2007-11

[14] Lenschow, D. H., and Stankov, B. B., "Length Scales in the Convective Boundary Layer," *Atmospheric Sciences Report*, Vol. 43, No. 12, 1986, pp. 1198–1209. doi:10.1175/1520-0469(1986)043<1198:LSITCB>2.0.CO;2

[15] Jarrin, N., Benhamadouche, S., Laurence, D., and Prosser, R., "A Synthetic-Eddy-Method for Generating Inflow Conditions for Large-Eddy Simulations," *International Journal of Heat and Fluid Flow*, Vol. 27, No. 4, 2006, pp. 585–593. doi:10.1016/j.ijheatfluidflow.2006.02.006

[16] Goedecke, G. H., Ostashev, V. E., Wilson, D. K., and Auvermann, "Quasi-Wavelet Model of Von kármán Spectrum of Turbulent Velocity Fluctuations," *Boundary-Layer Meteorology*, Vol. 112, No. 1, 2004, pp. 33–56. doi:10.1023/B:BOUN.0000020158.10053.ab

[17] Wilson, D. K., Ostashev, V. E., Goedecke, G. H., and Auvermann, H. J., "Quasi-Wavelet Calculations of Sound Scattering Behind Barriers," *Applied Acoustics*, Vol. 65, No. 6, 2004, pp. 605–627. doi:10.1016/j.apacoust.2003.11.009.

[18] Panofsky, H. A., and Dutton, J. A., *Atmospheric Turbulence*, Wiley, New York, 1983.

[19] Wilson, D. K., "A Turbulence Spectral Model for Sound Propagation in the Atmosphere that Incorporate Shear and Buoyancy Forcings," *Journal of the Acoustical Society of America*, Vol. 108, No. 5, 2000, pp. 2021–2038. doi:10.1121/1.1311779

[20] Sarpkaya, T., "New Model for Vortex Decay in the Atmosphere," *Journal of Aircraft*, Vol. 37, No. 1, 2000, pp. 53–61. doi:10.2514/2.2561

[21] Proctor, F., and Hamilton, D., "Evaluation of Fast-Time Wake Vortex Prediction Models," 47th AIAA Aerospace Sciences Meeting, Orlando, FL, AIAA Paper 2009-344, Jan. 2009.

[22] Garodz, L. J., and Clawson, K. L., "Vortex Wake Characteristics of B757-200 and B767-200 Aircraft Using the Tower Fly-By Technique," National Oceanic and Atmospheric Administration, TM Environmental Research Lab., Air Resources Lab., Rept. 199, Jan. 1993.

[23] Ash, R. L., and Zheng, Z. C., "Numerical Simulations of Commercial Aircraft Wakes Subjected to Airport Surface Weather Conditions," *Journal of Aircraft*, Vol. 35, No. 1, 1998, pp. 18–26. doi:10.2514/2.2284

[24] Zheng, Z. C., and Ash, R. L., "A Study of Aircraft Wake Vortex Behavior Near the Ground," *AIAA Journal*, Vol. 34, No. 3, 1996, pp. 580–589. doi:10.2514/3.13107

[25] Zheng, Z. C., and Baek, K., "Inviscid Interactions Between Wake Vortices and Shear Layers," *Journal of Aircraft*, Vol. 36, No. 2, 1999, pp. 477–480. doi:10.2514/2.2458

[26] Zheng, Z. C., and Lim, S. H., "Validation and Operation of a Vortex-Wake/Shear Interaction Model," *Journal of Aircraft*, Vol. 37, No. 6, 2000, pp. 1073–1078. doi:10.2514/2.2713

[27] Crow, S. C., "Stability Theory for a Pair of Trailing Vortices," *AIAA Journal*, Vol. 8, No. 12, 1970, pp. 2172–2179. doi:10.2514/3.6083

[28] Zheng, Z. C., "Thin-Tube Vortex Simulations for Sinusoidal Instability in a Counter-Rotating Vortex Pair," *International Journal for Numerical Methods in Fluids*, Vol. 39, No. 4, 2002, pp. 301–324. doi:10.1002/fld.327

[29] Li, W., Zheng, Z. C., and Xu, Y., "Flow/Acoustic Mechanisms in Three-Dimensional Vortices Undergoing Sinusoidal-Wave Instabilities," ASME 2007 International Mechanical Engineering Congress and Exposition, American Society of Mechanical Engineers, Paper IMECE2007-43163, Seattle, WA. Nov. 2007.